Astronomy & Astrophysics

The kinematics of water masers in the stellar molecular outflow source, IRAS 19134+2131

H. Imai[1,⋆], M. Morris[2], R. Sahai[3], K. Hachisuka[4,⋆⋆], and J. R. Azzollini F.[5,⋆⋆⋆]

[1] Joint Institute for VLBI in Europe, Postbus 2, 7990 AA Dwingeloo, The Netherlands
 e-mail: `imai@jive.nl`
[2] Department of Physics and Astronomy, University of California, Los Angeles, CA 90095−1562, USA
 e-mail: `morris@astro.ucla.edu`
[3] Jet Propulsion Laboratory, 4800 Oak Grove Drive, Pasadena, CA 91109, USA
 e-mail: `Raghvendra.Sahai@jpl.nasa.gov`
[4] Departamento de Astronomía, Universitat de Valéncia, 46100 Burjassot, Spain
 e-mail: `kazuya.hachisuka@uv.es`
[5] Instituto de Astrofísica de Canarias, La Laguna, Tenerife 38200, Spain
 e-mail: `jraf@cca.iac.es`

Abstract. Using the Very Large Array (VLA) and the Very Long Baseline Array (VLBA), we have observed water maser emission in the proto-planetary nebula candidate IRAS 19134+2131, in which the water maser spectrum has two groups of emission features separated in radial velocity by $\sim$100 km s^{-1}. The blue-shifted and red-shifted clusters of maser features are clearly separated spatially by $\sim$150 mas, indicative of a fast collimated flow. However, not all of the maser features are aligned along the axis of the flow, as is seen in the similar high-velocity water maser source, W43A. Comparing the VLA and VLBA maps of the water maser source, we find 4 maser features that were active for 2 years. Using only VLBA data, we identified proper motions for 8 maser features. The full 3D outflow velocity is estimated to be $\sim$130 km s^{-1}, indicating that the dynamical age of the flow is only $\sim$50 yr. On the basis of the relative positions with respect to the nearby extragalactic reference source, J1925+2106, we also obtain a secular motion of IRAS 19134+2131 of $\mu_l = -4.6 \pm 0.7$ mas yr^{-1} along the Galactic plane toward the Galactic centre. This indicates a "far distance" ($\geq$16 kpc) for IRAS 19134+2131 if the Galactic rotation curve remains flat at 220 km s^{-1}.

Key words. masers – stars: AGB and post-AGB – stars: distances – stars: kinematics – stars: winds, outflows – stars: individual: IRAS 19134+2131

1. Introduction

Stellar jets or fast flows have frequently been observed at the late as well as the earliest stages of stellar evolution. In particular, jets during late stellar evolution have been proposed to play an important role in shaping planetary nebulae, considering the frequent bipolarity/multipolarity and point-symmetry observed in proto-planetary and young planetary nebulae (PNe) (e.g., Sahai & Trauger 1998). The timing and the mechanism of jet formation, however, are still unclear because of the complexity of the final stages of stellar evolution. The circumstellar envelopes of AGB stars have roughly spherical morphologies and

slow expansion velocities (typically 10–20 km s^{-1}). However, these envelopes are transformed into proto-planetary nebulae (PPNe) with collimated fast ($>$100 km s^{-1}) outflows and complicated aspherical morphologies during a very short period of their post-AGB evolution ($\leq$1000 yrs, e.g. Lewis 2001).

We consider here a member of a small, but exceptionally interesting class of circumstellar water maser sources characterized by extremely large spreads of maser velocities (up to 260 km s^{-1}) (Likkel et al. 1992). This class of "water fountains" includes only three bona fide objects: IRAS 16342−3814 (hereafter IRAS 1634, Sahai et al. 1999; Morris et al. 2003), W43A (Imai et al. 2002, hereafter Paper I) and IRAS 19134+2131 (hereafter IRAS 1913). This class of sources appears to be closely related morphologically and kinematically to other post-AGB stars revealed by optical, infrared and mm-wave observations (e.g., OH 231.8+4.2). Although relatively high velocity OH masers ($V_{\rm exp} \sim 60$ km s^{-1}) exist in IRAS 1634 (Sahai et al. 1999), the water maser velocities are much higher. For W43A, Paper I described the discovery of a stellar jet traced by

water masers, which has a highly-collimated morphology and extreme kinematics and which exhibits precession. The water masers seem to delineate the locus of a bipolar precessing jet, whereas the OH masers are more broadly distributed in systemic latitude. Very likely the OH masers arise near the surface of an equatorial concentration of gas. Furthermore, the dynamical age of the jet is quite short ($\geq$40 yrs at present). Thus, the water fountains probably represent objects in a brief stage between a slow, spherical outflow and a fast axisymmetric outflow. Possibly, the jets in these systems have just been turned on, and they are now punching their ways through the spherical flows, carving out bipolar cavities as they go, and setting the stage for the formation of bipolar planetary nebulae.

Measurements of proper motions as well as radial velocities of water masers provide us the full three-dimensional velocity of a selected portion of the jets. If the source distance is known from other means, this yields the orientation of the jet major axis, which is important for developing a complete picture of the source geometry, including the radial distribution of dust. Unlike most well-studied post-AGB stars whose distances are reasonably well estimated, the distances to the water fountains are relatively unknown. However, if the maser proper motions are measured with respect to extragalactic reference sources, the kinematic distances can be well determined without the ambiguity that occurs when measuring only radial velocities of sources within the Solar circle of the Galaxy.

In this paper, we present the kinematics of water masers associated with IRAS 1913, as revealed by multi-epoch observations with the Very Large Array (VLA) and the Very Long Baseline Array (VLBA). Because the masers are too weak to apply self-calibration ($\leq$1 Jy) in the VLBA data and because we need to re-estimate the kinematic distance, we applied the phase-referencing mode to the VLBA observations. Section 2 describes in detail observations and data reduction using NRAO's AIPS software. Section 3 describes the results. Section 4 discusses the implications of the maser kinematics for the evolutionary status and the distances of the water fountains and for the outer Galactic kinematics.

2. Observations and data reduction

The VLA observation in the BnA configuration was made at 17:48–18:06 UT on 29 January 2001. The integration duration for IRAS 1913 was about 7 min. Two base-band channels (BBCs) in left circular polarization with a bandwidth of 3.125 MHz covered the blue-shifted and red-shifted maser components. The received signals were correlated and divided into 128 spectral channels in each of the BBCs, corresponding to a velocity spacing of 0.3 km s^{-1} in each of the spectral channels. 3C 295 was observed for the flux density scale and the complex bandpass calibration. The phase calibrator J1931+227 was observed for one minute twice and adopted as a position reference for IRAS 1913.

We did VLA data reduction with the normal procedure, applying self-calibration for the continuum calibrator. The flux density of 3C 295 was assumed to be 0.94 Jy at 22.2 GHz. We used a uniformly-weighted synthesized beam of 180 mas × 80 mas with a major axis at a position angle of −63°

to make image cubes. The detection limit was 0.16 Jy beam^{-1} at 5-σ noise level in a velocity channel without bright maser emission. Two types of image cubes of the IRAS 1913 masers were created; first with self-calibration using the maser data in a spectral channel at $V_{LSR} = -15.8$ km s^{-1} and second with phase-referencing using the data of J1931+227. The former image cube had better mapping quality because the phase fluctuations due to the atmosphere were well removed. Using the latter image cube, we obtained the absolute coordinates of the maser feature having a velocity of $V_{LSR} = -15.8$ km s^{-1}, $\alpha_{2000} = 19^h15^m35\overset{s}{.}2162 \pm 0\overset{s}{.}0003$, $\delta_{2000} = +21°36'33\overset{''}{.}916 \pm 0\overset{''}{.}003$.

The VLBA observations were made on 4 January and 7 March 2003 for a total of 10 h per epoch. NRAO 512 and J2148+0657 were observed for 6 min every 45 min for phase and bandpass calibration. The phase-referencing mode was adopted, in which each antenna nodded between the phase-reference and target maser sources in a period of 60 s. The on-source duration in each of the periods was shorter than 20 s depending on the target-reference separation and antenna zenith angle. J1910+2305 and J1925+2106 (hereafter J1925) were observed as phase-reference sources in different hour angles, but only J1925, ~2°5 away from IRAS 1913, was well detected in each of the periods. As a result, the effective coherent integration of the maser data was made for ~2.5 h. The received signals were recorded in 4 BBCs in dual circular polarization with a bandwidth of 4 MHz. Two of the BBCs covered the velocities of the red-shifted and blue-shifted maser components. The recorded data were correlated with the Socorro FX correlator in an integration period of 2 s. Each of the BBC data were divided into 256 spectral channels, corresponding to a velocity spacing of 0.2 km s^{-1} in each of the spectral channels. The following coordinates of IRAS 1913 were adopted in the data correlation: $\alpha_{2000} = 19^h15^m35\overset{s}{.}2150$, $\delta_{2000} = +21°36'33\overset{''}{.}900$.

In VLBA data reduction, we applied the procedures for the phase-referencing mode (e.g. Beasley & Conway 1995; Reid et al. 1999). First, residual delay/delay-rate solutions were obtained from fringe fitting for scans of NRAO 512 and J2148+0657. In this stage, we estimated that the residual delay solutions had uncertainties less than 3 nsec. Then fringe fitting was performed for scans of J1925. Most of the residual delay-rate solutions were smaller than 10 mHz; we could thus avoid 2π-n-radian ambiguity of fringe-phase interpolation between the successive calibrator scans. All of the calibration solutions obtained for J1925, including solutions in the self-calibration, were applied to the maser data. We used a naturally-weighted synthesized beam of 0.98 mas × 0.37 mas with a major axis at a position angle of −13° to make image cubes. The detection limit was 60 mJy beam^{-1} at 5-σ noise level in a velocity channel without bright maser emission.

The maser astrometry is affected by the brightness structure of J1925 and by relative difference in the excess path delays in the atmosphere between the reference and the maser sources due to different zenith angles. These are described in Appendices A and B. J1910+2305 was also marginally detected after applying fringe-fitting and self-calibration solutions for the maser data, but which is not described in detail here.
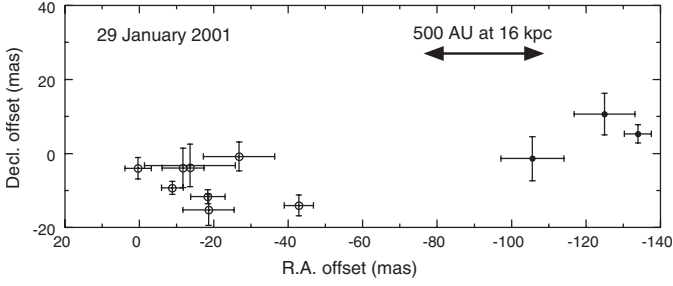
Fig. 1. Distribution of water maser features in IRAS 19134+2131 observed with the VLA. An uncertainty of a maser feature position is indicated by the size of a cross. The blue-shifted (-122 km s^{-1} $\leq$ $V_{\mathrm{LSR}} \leq -117$ km s^{-1}) and red-shifted (-37 km s^{-1} $\leq V_{\mathrm{LSR}} \leq$ -10 km s^{-1}) maser features with respect to the source systemic velocity, $V_{\mathrm{LSR}} = -67$ km s^{-1}, are shown in filled and opened circles, respectively.
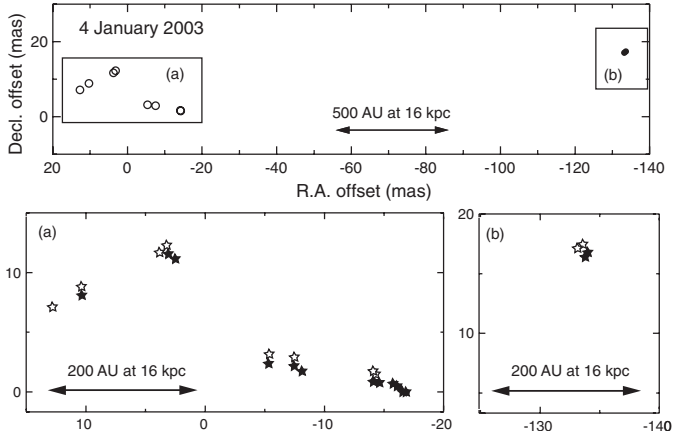

Fig. 2. Distributions of water maser features in IRAS 19134+2131 observed with the VLBA. *Upper*: radial velocity distribution of the maser features on 4 January 2003. The blue-shifted (-122 km s^{-1} $\leq$ $V_{\mathrm{LSR}} \leq -117$ km s^{-1}) and red-shifted (-37 km s^{-1} $\leq V_{\mathrm{LSR}} \leq$ -10 km s^{-1}) maser features with respect to the source systemic velocity, $V_{\mathrm{LSR}} = -67$ km s^{-1}, are shown in filled and opened circles, respectively. *Lower*: sub panels zooming up the blue-shifted **a)** and red-shifted **b)** clusters of maser features. Opened and filled stars indicate the feature locations on 4 January and 7 March in 2003, respectively.

3. Results

3.1. The IRAS 19134+2131 flow traced by water masers

Figures 1 and 2 show the distributions of the water maser features in IRAS 1913 observed with the VLA and the VLBA, respectively. Tables 1 and 2 give parameters of maser features detected with the VLA and the VLBA, respectively. The detection limits of the VLA and the VLBA observations were roughly equal to each other, and the maser distributions were roughly similar among the observations. Because of the large VLA synthesized beam and insufficient accuracy of maser feature positions, it is difficult to exactly trace the same maser features in the VLA and VLBA maps unless a maser feature is spatially isolated. Nevertheless, we found at least 4 maser

Table 1. Parameters of water maser features detected in the VLA observation.

V_{LSR} (km s^{-1})	$\Delta\alpha$ (mas)	$\Delta\delta$ (mas)	I_{Peak} (Jy beam^{-1})	$^{a}\Delta V$ (km s^{-1})
-118.9	-134 ± 4	5 ± 2	1.38	2.3
-115.3	-106 ± 8	-1 ± 6	0.22	0.2
-114.9	-125 ± 8	11 ± 6	0.34	0.7
-36.6	-43 ± 4	-14 ± 3	0.78	1.0
-21.5	-19 ± 7	-15 ± 4	0.41	1.7
-18.7	-27 ± 10	-1 ± 4	0.32	0.7
-17.0	-12 ± 6	-4 ± 5	1.16	1.3
$^{b}-15.9$	0 ± 4	-4 ± 3	1.77	1.7
-14.1	-14 ± 12	-3 ± 6	0.33	1.0
-13.2	-9 ± 3	-9 ± 2	1.11	1.0
-12.5	-18 ± 5	-12 ± 2	0.77	1.0

^{a} Full velocity coverage of the maser feature.
^{b} Maser feature containing the maser spot (located at the map origin) in the phase-reference velocity channel at $V_{\mathrm{LSR}} = -15.8$ km s^{-1}.

features that had been active for 2 years. The existence of maser features having lifetimes longer that one year is supported by the single-dish monitoring observations by Likkel et al. (1992), and helpful for high-precision measurements of maser proper motions.

The blue-shifted and red-shifted clusters of maser features are spatially well distinguished, indicating the existence of a collimated flow. The projected flow length is ~150 mas, corresponding to ~2400 AU at a distance of 16 kpc (see Sect. 4.2). Note that the VLA and VLBA observations did not reveal any straight line morphology in the maser feature clusters such as that seen in the W43A jet; the IRAS 1913 flow is thus less collimated than the W43A jet (Paper I). This is not a result of sensitivity bias for the detected maser features.

Using only VLBA data, we identified 8 proper motions of the water maser features (see Fig. 2 and Table 2). Note that, as described in Appendix A, the variation in the J1925 brightness structure introduces a coordinate drift of less than 15 μas. We measured at first mean proper motions of the blue-shifted and red-shifted clusters, then estimated a mean proper motion of the clusters as a secular motion that is discussed in the next section. An expansion motion of the flow is obtained as a relative motion of one of the two clusters with respect to the secular motion. Thus, we obtain an expansion rate of 1.5 ± 0.5 mas yr^{-1} in one direction in a position angle of about 74° east from north (weighted by the inverses of proper motion errors), corresponding to ~120 km s^{-1} on the sky plane. An uncertainty of the value was estimated from the standard deviation of the proper motions in two of the maser clusters. Combined with an expansion velocity of ~50 km s^{-1} along the line-of-sight, we obtain a 3D flow speed of ~130 km s^{-1}, an inclination of ~25° with respect to the sky plane, and a dynamical age of the flow of ~50 yrs assuming constant proper motions with time.

Table 2. Parameters of water maser features detected in the VLBA observations.

4 January 2003					7 March 2003					[b]Proper motion	
V_{LSR} (km s^{-1})	$\Delta\alpha$ (mas)	$\Delta\delta$ (mas)	I_{Peak} (Jy beam^{-1})	[a]ΔV (km s^{-1})	V_{LSR} (km s^{-1})	$\Delta\alpha$ (mas)	$\Delta\delta$ (mas)	I_{Peak} (Jy beam^{-1})	[a]ΔV (km s^{-1})	μ_α (mas yr^{-1})	μ_δ (mas yr^{-1})
−120.4	−133.54 ± 0.02	17.41 ± 0.04	0.32	1.9	−120.5	−134.01 ± 0.06	16.83 ± 0.15	0.05	0.6	−2.82 ± 0.06	−3.40 ± 0.16
−118.1	−133.19 ± 0.05	17.06 ± 0.08	0.22	1.7	−118.1	−133.72 ± 0.03	16.34 ± 0.05	0.11	1.1	−3.18 ± 0.06	−4.32 ± 0.09
−22.2	3.22 ± 0.07	12.30 ± 0.07	0.49	1.9	−22.1	3.13 ± 0.04	11.52 ± 0.05	0.31	1.5	−0.54 ± 0.07	−4.68 ± 0.09
...	...	...	...	...	−22.2	2.55 ± 0.03	11.09 ± 0.04	0.12	1.1	...	...
−20.6	3.85 ± 0.08	11.68 ± 0.18	0.08	0.8	...	...	...	...	...	...	...
−18.9	−14.24 ± 0.07	1.50 ± 0.04	0.13	1.1	−19.1	−14.11 ± 0.04	0.76 ± 0.05	0.10	0.6	0.78 ± 0.08	−4.48 ± 0.06
...	...	...	...	...	−18.0	−15.94 ± 0.06	0.39 ± 0.03	0.31	1.7	...	...
...	...	...	...	...	−17.9	−16.51 ± 0.02	−0.05 ± 0.04	0.13	0.8	...	...
−17.0	12.82 ± 0.05	7.14 ± 0.07	0.11	0.6	...	...	...	...	...	...	...
...	...	...	...	...	−16.9	−16.73 ± 0.05	−0.03 ± 0.05	0.13	0.8	...	...
...	...	...	...	...	−16.7	−16.15 ± 0.02	0.37 ± 0.02	0.28	0.8	...	...
...	...	...	...	...	−16.0	−16.26 ± 0.02	0.36 ± 0.04	0.28	1.1	...	...
...	...	...	...	...	−15.9	−16.85 ± 0.07	−0.04 ± 0.05	0.11	1.1	...	...
...	...	...	...	...	−15.8	−15.86 ± 0.12	0.57 ± 0.10	0.11	1.7	...	...
...	...	...	...	...	−15.4	−14.63 ± 0.05	0.82 ± 0.05	0.12	0.6	...	...
−14.8	10.40 ± 0.03	8.84 ± 0.02	0.33	0.8	−14.8	10.38 ± 0.02	8.04 ± 0.03	0.25	0.8	−0.12 ± 0.04	−6.40 ± 0.04
−14.0	−14.15 ± 0.01	1.66 ± 0.02	1.19	1.5	−13.9	−14.11 ± 0.02	0.89 ± 0.04	0.52	1.5	0.24 ± 0.02	−4.62 ± 0.04
−12.2	−5.34 ± 0.02	3.11 ± 0.03	0.19	0.8	−12.0	−5.27 ± 0.01	2.33 ± 0.04	0.20	0.8	0.42 ± 0.02	−4.68 ± 0.05
−11.1	−7.50 ± 0.01	2.87 ± 0.01	1.79	2.1	−11.1	−7.51 ± 0.01	2.10 ± 0.01	2.01	1.9	−0.06 ± 0.01	−4.62 ± 0.01
...	...	...	...	...	−11.1	−8.08 ± 0.01	1.69 ± 0.02	0.76	1.3	...	...

[a] Full velocity coverage of the maser feature.

[b] Errors contributing from thermal noise and feature structure are taken into account.

3.2. Galactic rotation at the IRAS 19134+2131 location

Adopting a mean motion between the blue-shifted and red-shifted clusters of maser features as the secular proper motion of the IRAS 1913 water maser source, we obtained this secular motion to be (weighted by inverses of proper motion errors),

$$\mu_\alpha = -1.5 \pm 0.2 \,(\pm 0.2) \text{ mas yr}^{-1},$$

$$\mu_\delta = -4.4 \pm 0.4 \,(\pm 0.2) \text{ mas yr}^{-1}.$$

The error in the parentheses indicates an expected systematic error. These equatorial velocity components are converted to Galactic coordinates as follows,

$$\mu_l = -4.6 \pm 0.7 \text{ mas yr}^{-1}, \quad \mu_b = -0.7 \pm 0.4 \text{ mas yr}^{-1}.$$

Thus, the secular motion is roughly along the Galactic plane toward the Galactic center, or dominated by Galactic rotation[1]. Since the radial velocity of IRAS 1913 is negative, we unambiguously conclude that it lies at a "far distance" rather than a "near distance". The far distance of IRAS 1913 is also consistent with its secular motion, which is smaller than that of Sgr A* at the Galactic center ($\mu_\alpha = -5.9$ mas yr^{-1}, Reid et al. 1999).

4. Discussion

4.1. What are the water fountains?

As described in Sect. 3.1, the IRAS 1913 flow, has similar physical parameters as those for another "water fountain",

the W43A jet, which has a projected length of ~1700 AU with an inclination of ≃39°, and a dynamical age of ~35 yrs in the year 1994[2] (Paper I). The IRAS 1634 flow is also similar: its projected length of the flow is ~4500 AU and the dynamical age is ≤100 yrs (Morris et al. 2003). Such a short time scale (≤100 yrs) of the three water fountains is consistent with their rarity; only these sources have velocity separations over 100 km s^{-1} (Likkel et al. 1992, see also the latest Arcetri catalog of water maser sources by Valdettaro et al. 2002).

These characteristics imply that highly collimated jets of molecular gas traced by water maser emission are seen only during such a short period. Moreover, strong collimation of a stellar jet might occur during much shorter time scale; only the W43A jet with the shortest dynamical age exhibits a strong collimation. The true morphology of the IRAS 1913 outflow, however, must be confirmed by detecting and following more maser features in order to examine these hypothesis. After all, a collimated jet of molecular gas traced by water maser emission is likely to quickly disappear after the above-mentioned time scale. We speculate that the jet has moved far enough out through the ambient, lower-velocity outflows so that the gas density is too low to excite maser activity in the high velocity jet by shocks (cf. Elitzur et al. 1989, 1992). This speculation is consistent with the observation of the PPN K3-35 (Miranda et al. 2001) in which a collimated jet traced by cm-wave radio continuum emission has a relatively long dynamical age of

[1] A possible effect of the annual parallax (<0.1 mas) is smaller than the proper motion uncertainty.

[2] In Paper I, the dynamical age of the W43A jet was incorrectly calculated, the projected length of the jet divided by the 3D jet speed. Here, the dynamical age is recalculated, the projected length divided by the projected jet speed.

~800 yrs, and only low-velocity water maser components are found.

There is a close alignment of the bipolarity axis in the optical image to the axis of the water maser jet in both IRAS 1634 (Morris et al. 2003) and IRAS 1913 (Sahai in private communication). This alignment strongly supports the idea that the operation of these jets has created the bipolar morphology in these objects. Thus, the water fountain nebulae are important objects for investigating the mechanisms involved in shaping planetary nebulae at their earliest stages. High spatial-resolution (interferometric) observations of CO emission from these objects, can further strengthen this hypothesis by enabling us to estimate the mass-loss rates and speeds of the molecular outflows and their correlations with the properties of the water fountain jets.

4.2. Implications for the source distance and Galactic-rotation velocity

The radial and transverse velocities of the source observed, V_r and V_t respectively, are expressed as follows,

$$V_r = \left(\frac{R_\odot}{R} V^{\mathrm{rot}} - V^{\mathrm{rot}}_\odot\right) \sin l \cos b + V_r^{\mathrm{pec}}, \tag{1}$$

$$V_t = a \mu_l r$$
$$= -\left[V^{\mathrm{rot}} \frac{r}{R} + \left(V^{\mathrm{rot}}_\odot - \frac{R_\odot}{R} V^{\mathrm{rot}}\right) \cos l\right] \cos b + V_{t,\parallel}^{\mathrm{pec}}, \tag{2}$$

where r is the heliocentric distance of the maser source in units of kiloparsecs, R and $R_\odot$ are the Galactocentric distances of the source and the Sun, V^{rot} and $V^{\mathrm{rot}}_\odot$ are the full Galactic rotation velocities at their locations, respectively, $a = 4.74$ km s^{-1} yr kpc^{-1} is the conversion factor from the measured proper motion to the transverse velocity, μ_l is the proper motion in units of mas yr^{-1} (see Sect. 3.2). V_r^{pec} and $V_{t,\parallel}^{\mathrm{pec}}$ are, respectively, the radial and transverse (parallel to the Galactic plane) components of a peculiar motion of the source, which are unknown and expressed as a deviation from circular Galactic rotation. The variables R and r are related:

$$R^2 = r^2 + R_\odot^2 - 2rR_\odot \cos l, \quad R > R_\odot. \tag{3}$$

From these equations, V^{rot} can be expressed in two forms as functions of R or r as follows,

$$V^{\mathrm{rot}} = \frac{R}{R_\odot}\left(\frac{V_r - V_r^{\mathrm{pec}}}{\sin l \cos b} + V^{\mathrm{rot}}_\odot\right), \tag{4}$$

$$V^{\mathrm{rot}} = -\left(a\mu_l R_\odot + V^{\mathrm{rot}}_\odot \cos b\right)\frac{R \cos l}{y \cos b}$$
$$-\frac{a\mu_l R}{\cos b} + \frac{R V_t^{\mathrm{pec},\parallel}}{y \cos b}, \tag{5}$$

where $y = \left(R^2 - R_\odot^2 \sin^2 l\right)^{1/2}$. $\tag{6}$

If the peculiar velocity components are known, then the solution for R and V^{rot} can be found by observing both a radial velocity and a proper motion for the maser source, and by assuming a Galactocentric distance to the Sun, $R_\odot = 8$ kpc, and a Galactic rotation velocity at the Sun, $V^{\mathrm{rot}}_\odot = 220$ km s^{-1}.
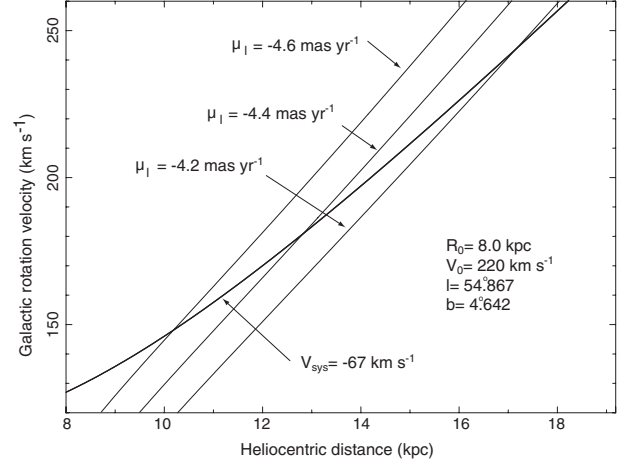

Fig. 3. Possible heliocentric distance, r, and Galactic rotation velocity, V^{rot}, of IRAS 19134+2131 located at $(l, b) = (54°867, 4°642)$. Three slopes of the function corresponding to the proper motions, $\mu_l = -4.6$, -4.4, -4.2 mas yr^{-1}, respectively, are plotted together with another curve corresponding to the source radial velocity $V_{\mathrm{LSR}} = -67$ km s^{-1}.

Figure 3 suggests that an accuracy of the proper motion better than 0.1 mas yr^{-1} is necessary to make a meaningful (r, V^{rot}) measurement. This accuracy is possible with current very long baseline interferometry (VLBI) techniques and with a longer time baseline of the monitoring observations. The source proper motion, $\mu_l = -4.6 \pm 0.7$ mas yr^{-1}, gives a Galactic rotation velocity at the source location, $V^{\mathrm{rot}} \sim 150$ km s^{-1} and a heliocentric distance of 10 kpc. Taking into account a possible flat Galactic rotation curve ($V^{\mathrm{rot}} = 220$ km s^{-1}), however, we obtain the values, $\mu_l \sim -4.2$ mas yr^{-1} and $r \sim 16$ kpc. To meaningfully perform the (r, V^{rot}) estimation, a μ_l-accuracy better than 0.1 mas yr^{-1} is essential. The source peculiar motion is also an unknown. In the Solar neighborhood, AGB stars have dispersions in the peculiar motions of $\sigma_r \simeq 22$ km s^{-1} and $\sigma_t \simeq 25$ km s^{-1} in the radial and transverse directions, respectively (Mihalas & Binney 1981). These dispersions cause uncertainties of up to 6 kpc and 60 km s^{-1} in a heliocentric distance and a Galactic rotation, respectively. At the outer Galaxy, a peculiar motion due to the Galactic warp is also expected (the warping disk traced by H I emission was recently well analyzed by Nakanishi & Sofue 2003).

Nevertheless, the analyses described above are still useful to elucidate the outer Galactic rotation curve and the source location in the Galaxy. Future statistical analyses may reveal a mean Galactic rotation curve based on the kinematics of a group of AGB/post-AGB stars and stellar peculiar motions can be determined as deviations from the mean Galactic rotation.

5. Summary

The present VLA and VLBA observations have revealed the distribution and the kinematics of the water masers in IRAS 1913 and the secular motion of IRAS 1913 following the Galactic rotation. The existence of a well-collimated flow is supported by the blue-shifted and red-shifted maser components that are well spatially separated. The measured flow length of 150 mas and its expansion rate of ~1.6 mas yr^{-1} give

a flow dynamical age of ~50 yrs. Compared with the jet parameters of other "water fountains", W43A and IRAS 1634, and rarity of this kind of objects, we speculate that the water fountains are seen during a very short period (≤100 yrs). It is most likely that, after this time, the aligned high-velocity water maser features disappear and only the low-velocity components of water maser emission exist, until eventual photoionization of the circumstellar envelope. The secular motion of IRAS 1913 along the Galactic plane, $\mu_l \sim -4.6$ mas yr^{-1}, puts IRAS 1913 at a "far distance" (~10 kpc depending on the Galactic rotation curve). More accurate measurements of the IRAS 1913 secular motion and those of similar, distant objects will enable us to estimate not only the distance to these objects but also the outer Galactic rotation curve and interesting characteristics in their peculiar motions. Long-term activity of individual maser features over 2 yrs should support such measurements.

Appendix A: The brightness structure of the J1925+2106

The celestial coordinates for the IRAS 1913 water masers in this paper are well fixed by the extragalactic reference frame using the reference source J1925. Figure A.1 shows the brightness structure of J1925 at the two epochs – a bright core, very close to the map origin (component *A*), and one or two more fainter components, are visible. The second brightest component (component *B*) is located at a position angle of about −100° from north with respect to component *A*, which is consistent with the direction of the elongated distribution of radio emission components seen in longer wavelength bands (e.g., Fomalont et al. 2000). Because the self-calibration process puts the coordinate origin at the mean center of the J1925 brightness structure, the stability of the coordinates depends on the time variation of the J1925 brightness structure.

Table A.1 gives the locations of components *A* and *B*, which were estimated by Gaussian model fitting using the AIPS task JMFIT. Component *A* is offset by ~40 μas from the map origin, but has been stable within ~6 μas between the two epochs. This component, likely associated with a massive black hole, is suitable as a position reference for the astrometry of the IRAS 1913 masers. On the other hand, component *B* may exhibit a proper motion of 108 ± 140 μas. This motion will be better estimated by additional observations covering a longer time interval (≤1 yr). The third brightest component was marginally seen to the west of the brightest component, but its proper motion appears abnormally large (~3 mas yr^{-1}). We judge that the significance of this result is still low.

The coordinates are also affected by the parameters adopted in data reduction. We performed the model fitting by adopting models having two elliptical Gaussian features for components *A* and *B*. We prepared three maps with different pixel
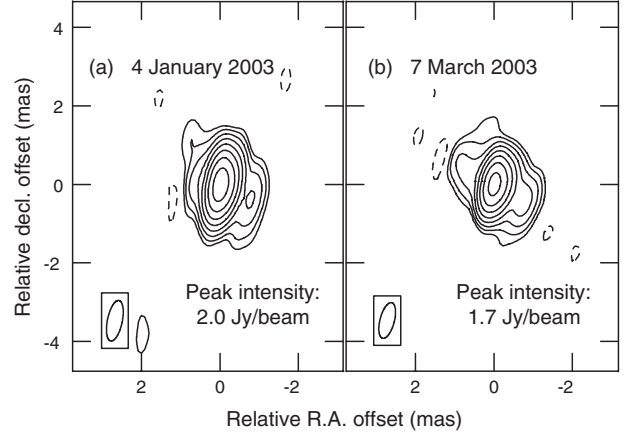

Fig. A.1. Brightness distribution of J1925+2106 at the first **a)** and second **b)** epochs. The contour levels are set at −10, 10, 20, 40, 80, 160, 320, 640 and 1280 mJy beam^{-1}. A box in the left-bottom corner indicates the synthesized beam.

Table A.1. Locations of the two brightness components in J1925+2106.

Comp.	Relative offsets on 4 Jan. 2003		Difference between 7 Mar. and 4 Jan.	
	$\Delta\alpha$ (μas)	$\Delta\delta$ (μas)	$\Delta\alpha$ (μas)	$\Delta\delta$ (μas)
A	−28 ± 7	−22 ± 6	5 ± 10	12 ± 7
B	−454 ± 89	−12 ± 101	−31 ± 104	−94 ± 119

sizes and performed the fitting many times by changing fit field sizes and a-priori locations of the two components. The standard deviations of the estimated component locations should correspond to uncertainties in the locations, which are given in Table A.1. Thus we conclude that the assumption of coordinate stability is uncertain by ≤15 μas because of brightness frame variation.

Appendix B: Astrometric error due to different excess path delays between two sources

In contrast to relative proper motions among maser features, proper motions with respect to a reference source, a few degrees away from the maser source, have worse accuracies because of additional errors in measured relative phase delays due to the unknown difference of atmospheric excess path delays between the two sources. For the VLBA data, this additional phase-delay error, $\Delta\tau$, was evaluated by Reid et al. (1999) using the following equation,

$$\Delta\tau \approx \tau_0 \sec Z \tan Z \Delta Z, \tag{B.1}$$

where $\tau_0 \sim 0.1$ ns is the phase-delay error at the zenith yielded in the VLBA correlation model, Z the zenith angle of the one of the two observed sources, ΔZ the zenith angle difference between the two observed sources. In the present paper adopting $Z \sim 30°$, $\Delta Z \sim 2.5°$, a typical phase-delay error of about 2.2×10^{-12} s is obtained, which corresponds to a position error

of 130 μas when observing with a 1000-km baseline. Thus a systematic error of the order of 100 μas is expected.

References

Beasley, J. A., & Conway, J. E. 1995, Very Long Baseline Interferometry and the VLBA, ed. J. A. Zensus, P. J. Diamond, & P. J. Napier (San Francisco: ASP), ASP Conf. Ser., 82, 328

Fomalont, E. B., Frey, S., Paragi, Z., et al. 2000, ApJS, 131, 95

Elitzur, M., Hollenbach, D. J., & McKee, C. F. 1992, ApJ, 394, 221

Elitzur, M., Hollenbach, D. J., & McKee, C. F. 1989, ApJ, 346, 983

Imai, H., Obara, K., Diamond, P. J., Omodaka, T., & Sasao, T. 2002, Nature, 417, 829

Lewis, B. M. 2001, A&A, 560, 400

Likkel, L., Morris, M., & Maddalena, R. J. 1992, A&A, 256, 581

Mihalas, D., & Binney, J. 1981, Galactic Astronomy, second edition, Structure and Kinematics (San Francisco: W. H. Freeman and Company), Chap. 7

Miranda, L. F., Gómez, Y., Anglada, G., & Torrelles, J. M. 2001, Nature, 414, 284

Morris, M. R., Sahai, R., & Claussen, M. 2003, RMxAC, 15, 20

Nakanishi, H., & Sofue, Y. 2003, PASJ, 55, 191

Reid, M. J., Readhead, A. C. S., Vermeulen, R. C., & Treuhaft, R. N. 1999, ApJ, 524, 816

Sahai, R., Te Lintel Hellert, P., Morris, M., Zijlstra, A., & Likkel, L. 1999, ApJ, 514, L115

Sahai, R., & Trauger, J. T. 1998, AJ, 116, 1357

Valdettaro, R., Palla, F., Brand, J., et al. 2002, A&A, 368, 845